European Journal of Medicinal Chemistry 304 (2026) 118504

Contents lists available at ScienceDirect

European Journal of Medicinal Chemistry

journal homepage: www.elsevier.com/locate/ejmech

Research paper

Ketoconazole-carbonic anhydrase inhibitors as potential anticancer agents

Elena Andreucci [a], Alessio Biagioni [a,*], Sara Peri [a], Nunzia Di Menna [b], Michela Pinto [a], Serena Martinelli [b], Laura Papucci [a,**], Lucia Magnelli [a], Gioele Renzi [c], Silvia Selleri [c], Andrea Angeli [c], Clemente Capasso [d], Fabrizio Carta [c,***], Claudiu T. Supuran [c]

[a] Department of Experimental and Clinical Biomedical Sciences, Università degli Studi di Firenze, 50134, Florence, Italy
[b] Department of Experimental and Clinical Medicine, Università degli Studi di Firenze, Florence, 50134, Italy
[c] Università degli Studi di Firenze, NEUROFARBA Department, Section of Pharmaceutical and Nutraceutical Sciences, Via Ugo Schiff 6, Sesto Fiorentino, Florence, 50019, Italy
[d] Department of Biology, Agriculture and Food Sciences, Institute of Biosciences and Bioresources, Napoli, 80131, Italy

ARTICLE INFO

Keywords:
Carbonic anhydrase inhibitors
Extracellular vesicles
Tumors

ABSTRACT

The biochemical complexity of cancers offers the possibility to repurpose known drugs for new therapeutic applications. In this study, we exploited the potential anticancer effects of a series of compounds structurally organized with the tumor-associated Carbonic Anhydrase (CA; EC 4.2.1.1) IX/XII inhibiting warhead and the antifungal drug Ketoconazole (KTZ), which was recently considered in oncology for its ability to suppress steroidogenesis as well as disruption of the biogenesis of extracellular vesicles (EVs). The data here reported gives the first line of evidence that the *in vitro* antiproliferative effects of such compounds on a panel of tumoral cell lines are ascribed to integration of the anti-CA IX/XII effect with the EV pathway disruption and thus might represent a promising dual-mechanism therapeutic approach.

1. Introduction

One of the hallmarks of cancer is its ability to adapt to harsh microenvironmental conditions [1] and hijack intercellular communication pathways [2] to promote proliferation, invasion, and metastasis. In this context, targeting pH regulation in tumor cells [3] and disrupting the intercellular communication [4], commonly mediated by extracellular vesicles (EVs) [5], might represent a new and efficient way to treat cancers [2]. A defining feature of many solid tumors is the acidic extracellular (pH*e*) generated by an advanced anaerobic glycolysis, coupled with a neutral or alkaline intracellular pH (pH*i*) [1,6]. This pH gradient, largely due to the Warburg effect and poor perfusion leading to hypoxia, is fundamental for cancer cell survival and invasiveness [1,3,6]· [7]. The metalloenzyme Carbonic Anhydrases IX and XII (CAs IX/XII; EC 4.2.1.1) are key mediators of pH homeostasis and are typically overexpressed in a wide variety of human cancers, being actively involved in maintaining favorable pH*i* while simultaneously contributing to the acidic pH*e* that promotes extracellular matrix degradation, immune evasion, and chemotherapy resistance [3,6,8–11]. The biochemical complexity of cancers offers several advantages, such as the pharmacological repositioning of known drugs used for different therapeutic applications [12]. Examples of this kind are the antifungal drugs of the azole type [13], which among others include the Ketoconazole (**KTZ**) repurposed in oncology for its disrupting effects on steroidogenesis [13]. Growing evidences indicate that **KTZ** itself or its metabolic derivatives may exert direct anti-cancer effects through multiple mechanisms, several of which are still unknown [13]. Particularly relevant for this work, is the ability of **KTZ** to suppress EVs biogenesis and secretion by affecting the pathways critical for their formation, such as the Endosomal Sorting Complexes Required for Transport (ESCRT) machinery [14]. EVs are a heterogeneous family of lipid bilayer-enclosed nanoparticles naturally released by all kinds of cells into the extracellular milieu [15]. This large family includes exosomes, microvesicles, and apoptotic bodies, and is commonly classified

Abbreviations: CA, Carbonic Anhydrase; CAI, Carbonic Anhydrase Inhibitor; ESCRT, Endosomal Sorting Complexes Required for Transport; EVs, extracellular vesicles.

* Corresponding author.
** Corresponding author.
*** Corresponding author.
E-mail addresses: alessio.biagioni@unifi.it (A. Biagioni), laura.papucci@unifi.it (L. Papucci), fabrizio.carta@unifi.it (F. Carta).

https://doi.org/10.1016/j.ejmech.2025.118504
Received 6 November 2025; Received in revised form 12 December 2025; Accepted 15 December 2025
Available online 17 December 2025

by the diameter into small and large EVs [16]. EVs serve as crucial mediators of intercellular communication, acting as biological messengers by packaging and transferring bioactive cargo including proteins, lipids, mRNAs, and miRNAs to distant recipient cells [2,4,5,16]. In cancers, the EV mediated communication is amplified and hijacked by tumor cells to stimulate angiogenesis, to establish an immunosuppressive microenvironment, to facilitate pre-metastatic niche formation, and to promote drug resistance through the export of chemotherapeutic agents or the transfer of signaling effectors [17]. In fact, EV levels are elevated in cancer cells, providing further evidence of their correlation with tumor burden and metastatic potential [15].

In this work, we assessed the role of small molecule compounds constituted by the **KTZ** drug linked to inhibitors of the CAs IX and XII with the intent to disrupt simultaneously the pH-regulating machinery and the EV-mediated communication in cancer cells.

2. Results and discussion

2.1. Design and synthesis of compounds

In line with the proof of concept nature of this work we did make use of a linear synthetic approach to connect the piperazine tail of **KTZ** to prototypic CAI warheads of the primary sulfonamide and coumarin types as in Fig. 1 [18].

Such a synthetic approach proved ideal for building up a library of investigational compounds featured with the pharmacophoric groups well exposed [18], and therefore ready to interact with the corresponding biochemical targets. The same was applied to the synthesis of the coumarin-containing derivatives **3a-d** in Scheme 1 here reported for the first time.

All final compounds were purified by silica gel column chromatography using the appropriate eluting mixtures and followed by trituration or recrystallization as needed (see experimental section). Full characterization was conducted by means of solution ^{1}H, ^{13}C NMR. Elemental analyses account for a purity grade ≥96 %.

2.2. Carbonic anhydrase in vitro enzymatic assay

The **KTZ** containing compounds of the sulfonamide type (i.e. **4, 5a-d**, **6a-b**, **7a-d**, **8**–**10**, **11a-c**, **12a-c**, **13a-c**, **14**, **15**, **16a-d** and **17a-d** in Fig. 2) [18] and the newly reported **3a-d** were screened *in vitro* through the stopped-flow CO_2 hydrase assay [19] to assess their inhibitory activity and selectivity profiles on hCAs I, II, IX and XII. The data obtained are all reported in Table 1 as K_I values and are compared to the primary sulfonamide drug Acetazolamide (**AAZ**) and coumarin (**COU**) as reference compounds.

Structure-activity relationships (SARs) relative to **3a-d** on hCAs I, II, IX and XII are discussed below. As for the remaining compounds in Table 1, pertinent SAR considerations have already been thoroughly addressed in our previous study [18]. For sake of clarity, it is enough to remind that they all accounted for the transmembrane and tumor-associated CAs being preferentially inhibited over the constitutive and largely expressed I and II isoforms. Noteworthy, data in Table 1 clearly showed that compounds **3a-d** exerted preferential inhibition of the tumor-associated hCAs IX and XII and thus retained the kinetic trend of the previously explored **KTZ**-sulfonamide derivatives [12]. Specifically, among the **3a-c** series, introduction of the trifluoromethyl (i.e. **3b**) and methyl (i.e. **3c**) moiety at the 4-position of the coumarin ring progressively enhanced the inhibition potency for the hCA I up to 3.0-fold (Table 1). As for the hCA II isoform, the trifluoromethyl derivative **3b** was the best performing inhibitor with a K_I value of 7.36 μM, whereas the 4-mehyl substituted **3c** and the unsubstituted **3a** were almost equipotent (i.e. K_Is of 27.1 and 35.5 μM for **3a** and **3c,** respectively). A palindromic-like trend was observed for the kinetic values of **3a-c** relative to the tumor-associated hCAs IX and XII (Table 1). For instance, **3a** was a 474.0 nM hCA IX inhibitor and the 4-substituted coumarinyl **3b** and **3c** were perfectly matching being the associated K_I values of 75.0 and 74.0 nM respectively. As for the XII isoform, K_Is of 96.0 and 97.0 nM were reported for compounds **3a** and **3b**, whereas **3c** was effective at 302.0 nM (Table 1). Among all compounds screened and reported in Table 1, the derivative **3d** was the least potent on the hCA I (i.e. K_I of 25.7 μM) and comparable to the hCA II (i.e. K_I of 27.4 μM). This last value is perfectly aligned with that of **3a** on the same isoform (Table 1). Noteworthy **3d** is equipotent to **3b** and **3c** on the hCA IX (i.e. K_I of 74.0 nM) and to **3a** and **3b** for the hCA XII (i.e. K_I of 92.0 nM).

2.3. Anti-proliferative activity in human cancer cells in vitro

Based on *in vitro* enzymatic profiles and solubility features, compounds **3c** and **17d** were further considered for their ability to impair cancer cells' proliferation *in vitro*. Specifically, we focused on derivatives containing either the primary sulfonamide moiety (e.g., **17d**) or the coumarin ring (e.g., **3c**), as these structures preferentially inhibit the CA IX and CA XII isoforms. Our aim was to assess whether such selective inhibition could differentially influence the outcomes of cellular proliferation assays on cancer cell lines of different origins, such as clear cell renal cell carcinoma -ccRC- (Caki-1, 786-O), pancreatic ductal adenocarcinoma -PDAC- (MIA PaCa-2, PANC-1), gastric adenocarcinoma -GC- (ACC-201, MKN-74), breast carcinoma -BC- (MCF-7, MDA-MB-231), and cutaneous melanoma -CM- (A375, 501Mel). All cell lines tested clearly showed high expression of the tumor-associated CA IX and CA XII as in agreement with the literature [8–11]. Specifically, Fig. 3A reports the representative images of the CA IX and CA XII immunofluorescence staining in green in the upper and lower panel, respectively. A noticeably stronger green fluorescence signal was observed in the CA IX–related images compared to those of CA XII. In contrast, in most of the CA XII images, the blue fluorescence corresponding to nuclear DAPI staining was predominant. Similarly, In-Cell Western assay in Fig. 3B,

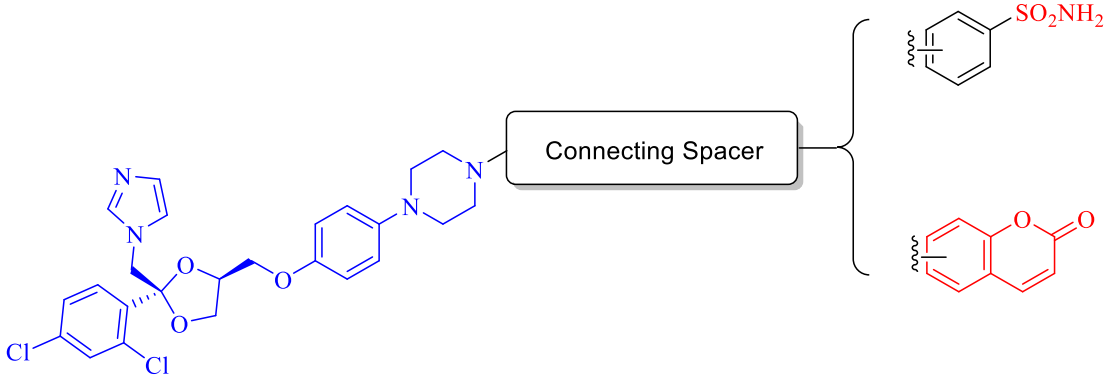

Fig. 1. Schematic representation of the **KTZ**-CAI compounds reported in this study.

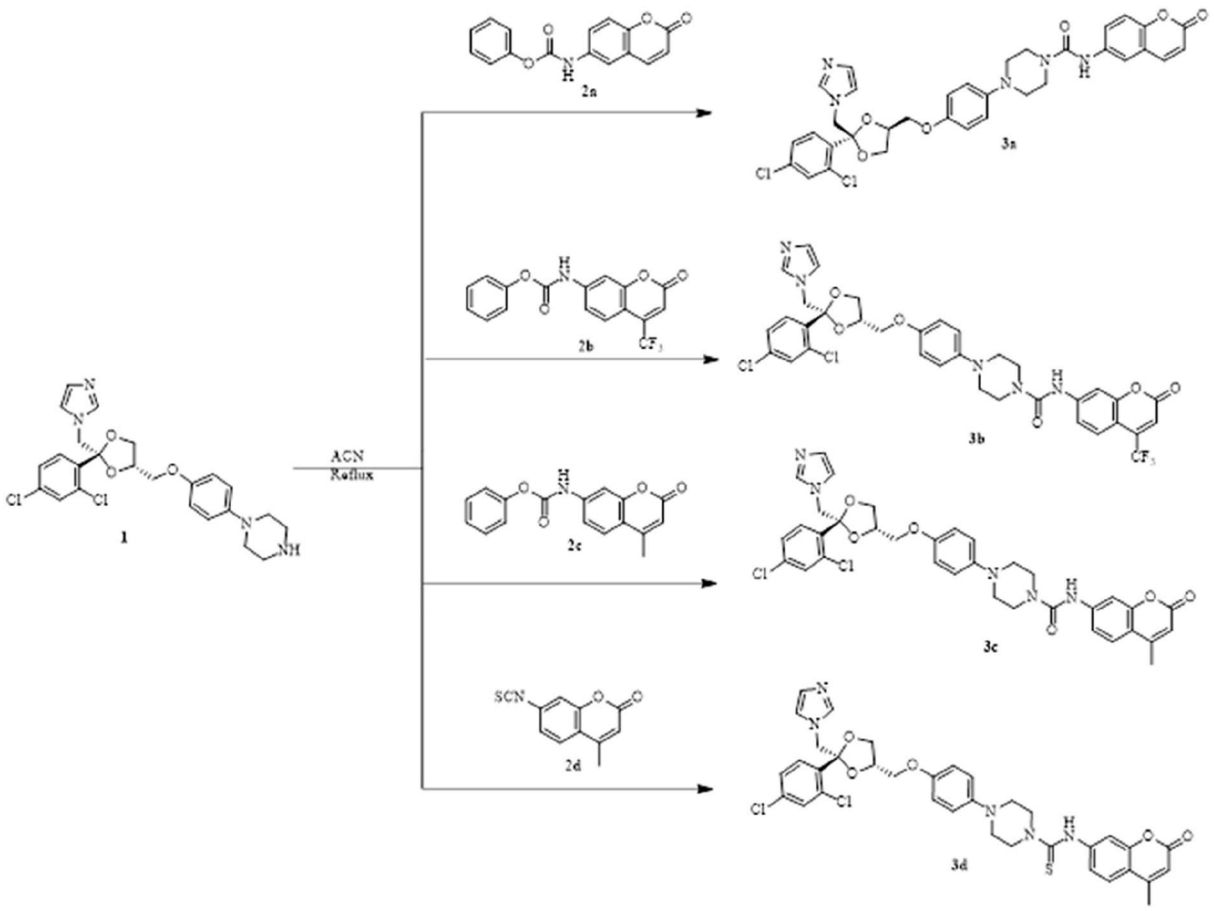

Scheme 1. Synthesis of compounds **3a-d**.

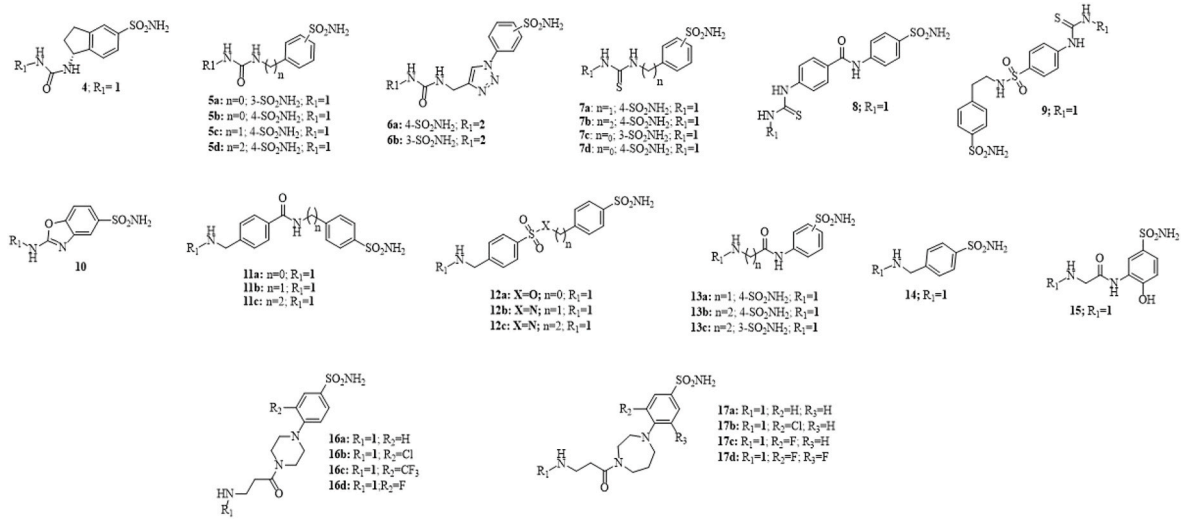

Fig. 2. Chemical structure of compounds **4, 5a-d**, **6a-b**, **7a-d**, **8**–**10**, **11a-c**, **12a-c**, **13a-c**, **14**, **15**, **16a-d** and **17a-d**.

revealed a basal co-expression of CA IX and CA XII by all the cell lines tested, with again a significant predominance of CA IX over CA XII.

After confirming that all cancer cell lines expressed detectable yet variable levels of both CA IX and CA XII, we used these models to evaluate the inhibitory activity of compounds **3c** and **17d**. Cell proliferation was assessed using the MTT assay 72 h after the initiation of treatment with increasing concentrations of compounds **3c** and **17d**. Derivative **3c** was unable to affect the proliferation of the ccRCC Caki-1 and 786-O cells, as well as the PDAC MIA PaCa-2 and PANC-1 cells, even at the maximum dose used (IC_{50} > 100 μM) (Fig. 4). Compound **3c** showed instead an inhibition activity on GC cell proliferation with IC_{50} of 12.80 μM and 10.17 μM for ACC-201 and MKN-74 cells, respectively (Fig. 4). Similarly, on CM A375 cells, **3c** showed an IC_{50} of 9.76 μM, while no proliferation impairment was observed on the second CM cell line 501Mel (IC_{50} > 100 μM) (Fig. 4). In the BC MDA-MB-231 cells, **3c** showed a marked anti-proliferation activity, with IC_{50} being 1.826 μM,

Table 1
Inhibition data of compounds **3a-d, 4, 5a-d**, **6a-b**, **7a-d**, **8**–**10**, **11a-c**, **12a-c**, **13a-c**, **14**, **15**, **16a-d** and **17a-d** on hCAs I, II, IX and XII. **AAZ** and **COU** were considered as references. [19].

Compound	K_I (nM)[a,b]			
	hCA I	hCA II	hCA IX	hCA XII
3a	2190	27080	474.0	96.0
3b	1790	7360	75.0	97.0
3c	740.0	35500	74.0	302.0
3d	25720	27410	74.0	92.0
4	5912	5847	4.4	63.1
5a	1622	1864	15.1	39.6
5b	337.6	71.8	32.9	8.2
5c	437.2	58.9	13.9	6.4
5d	84.0	563.4	6.0	9.5
6a	870.2	390.0	38.0	44.0
6b	896.5	533.9	41.2	7.4
7a	862.9	605.0	47.7	72.5
7b	871.7	258.0	48.7	9.2
7c	328.2	392.9	40.1	8.0
7d	861.0	736.6	4.4	8.2
8	871.5	882.6	41.0	9.0
9	58.3	17.3	151.8	62.3
10	944.0	8.3	28.3	47.2
11a	352.5	26.5	46.8	8.2
11b	4767	620.0	368.6	64.4
11c	5515	55.7	47.9	7.5
12a	2662	180.0	311.5	5.9
12b	3418	1196	41.9	6.2
12c	2986	938.8	43.9	8.1
13a	497.4	21.4	346.3	61.0
13b	9238	798.6	49.1	9.1
13c	4351	92.6	331.4	9.4
14	382.0	122.0	224.8	9.3
15	817.8	77.1	76.0	6.3
16a	82.1	49.1	30.6	3.7
16b	769.7	20.7	48.4	31.1
16c	835.8	167.9	445.7	9.4
16d	363.9	44.6	306.3	56.1
17a	315.1	288.5	13.8	5.5
17b	96.1	195.6	272.1	67.9
17c	5.3	7.2	284.6	7.9
17d	777.0	247.4	2167	55.9
AAZ	250.0	12.1	25.8	5.7
COU	3100	9200	>100000	>100000

[a] Mean from 3 different assays, by the stopped flow technique (errors were in the range of ± 5–10 % of the reported values).
[b] K_I values of **3a-d** are reported here for the first time, whereas the remaining compounds were in the literature [18].

but no activity was detected on the MCF-7 BC cells (IC_{50} > 100 μM) (Fig. 4).

Compared to **3c**, the derivative **17d** showed marked anti-tumor activity (Fig. 5). Specifically, compound **17d** demonstrated potent anti-proliferative effects across most of the tested lines. On ccRCC, the IC_{50} of **17d** was observed at sub-micromolar concentration in Caki-1 cells (IC_{50} = 0.79 μM), and 2.76 μM in 786-O cells (Fig. 5). When tested on PDAC cells, we observed a IC_{50} of 3.53 μM in MIAPaCa-2 cells, while in the PANC-1 cell line a clear IC_{50} was not attained within the tested concentration range, then estimated to be greater than 100 μM (Fig. 5). This suggests that PANC-1 cells may possess an inherent or induced resistance mechanism to **17d**. In GC cells, **17d** showed an IC_{50} of 1.86 μM for ACC-201 cells and 2.91 μM for MKN-74. In the CM models tested, higher IC_{50}s were observed, but still significantly lower than **3c** (Fig. 5). In the triple negative BC model of MDA-MB-231 cells, **17d** reached an IC_{50} of 0.953 μM, while on the ER + MCF7 cell line the IC_{50} was higher (i.e., 3.89 μM) but still lower that that relative to the **3c** derivative (Fig. 5).

Importantly, the analysis of both compounds (**3c** and **17d** in Fig. 6A and B**,** respectively) in human umbilical vein endothelial cells (HUVEC) and normal human dermal fibroblasts (NHDF) revealed their lack of anti-proliferative activity, indicating that they do not affect the viability of non-tumor/healthy cell lines.

2.4. Compound 17d inhibits EV secretion

Based on the superior anti-proliferative activity of **17d** over **3c,** we determined whether the former affected EV secretion/production. Specifically, we quantified EVs in tumor cells, including renal (Caki-1), melanoma (A375 and 501Mel), and breast (MDA-MB-231). EVs were isolated from conditioned medium as described in the Experimental section, normalized to cell number, and the results were expressed as the ratio of EVs per cell in **17d**-treated samples relative to vehicle-treated controls (Veh = 1). As shown in Fig. 7A, the tested compound **17d** was capable of significantly reducing EV secretion/production in all the cell lines. Moreover, as shown in Fig. 7B, treatment with **17d** also led to a significant increase in the D90 value for 501Mel and Caki-1, thus suggesting a modest enrichment in larger EVs within the upper percentile of the size distribution.

3. Conclusions

Herein, we report the validation of **KTZ** derivatives bearing the CAI warheads of the primary sulfonamide and coumarin types as potential tools for the management of tumors. Among the set of compounds considered in this study, the coumarin derivatives **3a-d** were described for the first time. Overall, *in vitro* inhibition data on the hCAs I, II, IX and XII accounted for the inhibitors having preferential binding for the tumor-associated isoforms (i.e. IX and XII) with K_I values comprised in the low-medium nanomolar range.

Selected compounds **3c** and **17d** were further considered for their ability to decrease proliferation in tumor cell lines. Screening of selected compounds revealed a marked difference in cellular efficacy. Compound **17d** exhibited significantly superior anti-proliferative activity compared to **3c**, and was highly potent, achieving a sub-micromolar IC_{50} of 0.79 μM on ccRCC Caki-1 cells and exhibiting significant effects across most tested cancer lines. This differential effect suggests that the specific CA warhead structure (coumarin *vs* sulfonamide) significantly influences the overall cellular potency of the **KTZ**-conjugate. Importantly, both compounds showed no anti-proliferative activity on normal cell lines, such as the endothelial and fibroblastic cell models tested in this study. Moreover, **17d** compound also demonstrated the capacity to significantly suppress EV secretion in ccRCC Caki-1 cells, CM A375 and 501Mel cells, and BC MDA-MB-231 cells, which is a key mechanism of **KTZ**'s anti-cancer action [13,14]. In drug-treated samples, NTA analysis revealed that the significant reduction in the total number of EVs was accompanied by an increase in the D90 compared to controls. This shift toward larger particle sizes is likely related to the reduced cell viability observed under the same experimental conditions, suggesting that, in addition to inhibiting the biogenesis of smaller vesicles, the treatment may promote the release or co-isolation of larger particles such as microvesicles or apoptotic bodies.

Collectively, these findings demonstrate that the **17d** derivative successfully integrates the anti-CA IX/XII effect with the EV pathway disruption attributed to the KTZ moiety. By simultaneously targeting tumor pH regulation and intercellular communication via EVs, **17d** might represent a promising dual-mechanism therapeutic candidate. Future studies should focus on elucidating the precise molecular mechanism by which the CA inhibition enhances the EV suppression activity and evaluating the compound's efficacy in relevant *in vivo* models.

4. Experimental section

4.1. Chemistry

Anhydrous solvents and all reagents were purchased from Sigma-Aldrich, Alfa Aesar and Fluorochem. All reactions involving air- or

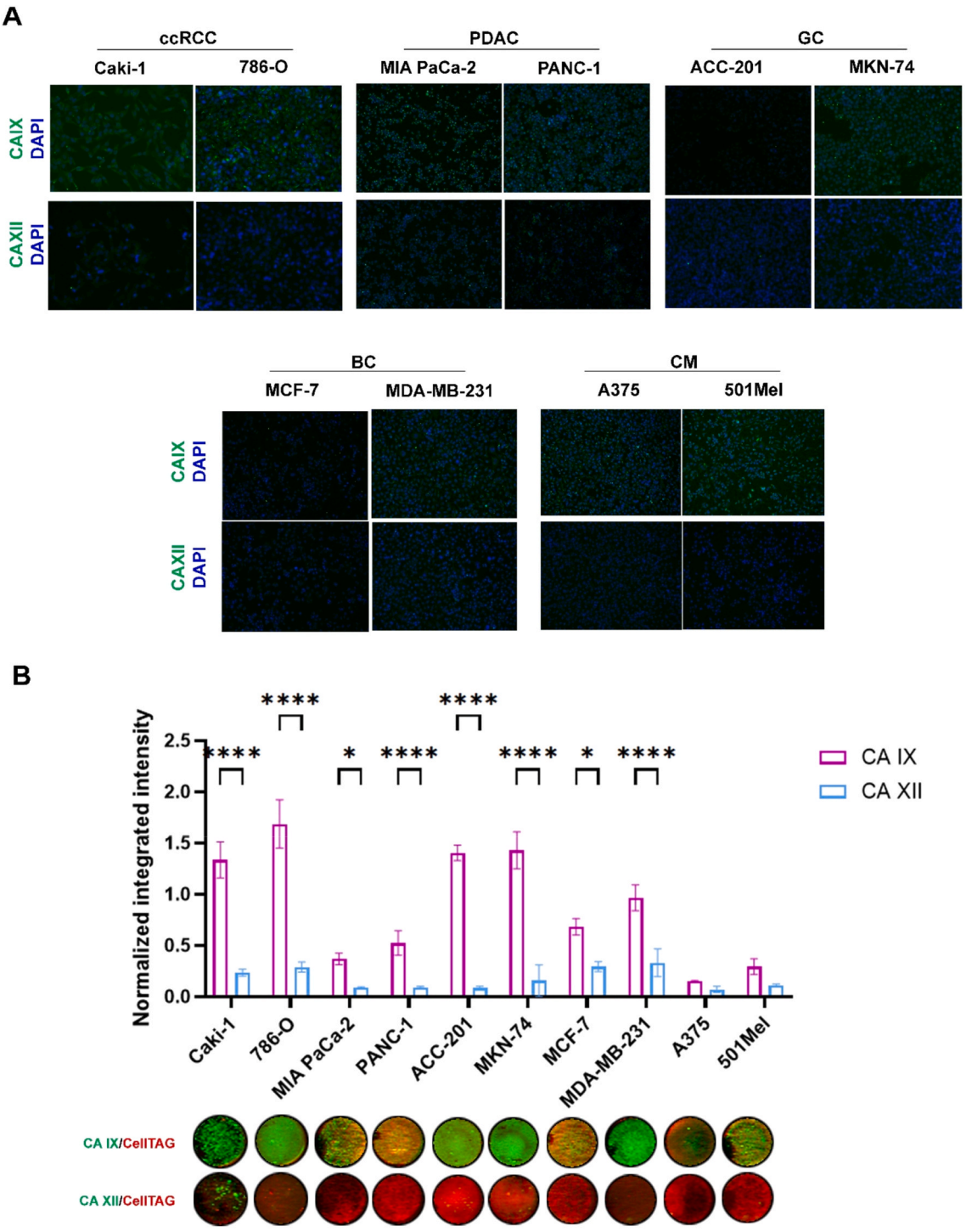

Fig. 3. **A**) Immunofluorescence staining of CA IX and XII in green over nuclei staining in blue (DAPI) (10x magnification) – ccRCC: clear cell Renal Cell Carcinoma; PDAC: Pancreatic Ductal Adenocarcinoma; GC: Gastric Cancer; BC: Breast Cancer; CM: Cutaneous Melanoma. **B**) Quantification chart of the In-Cell Western fluorescence analysis of CA IX and CA XII (upper panel), and relative representative images of their fluorescent signal in green over red, Cell TAG used for internal normalization. *$p < 0.05$, ****$p < 0.0001$, Two-way ANOVA, GraphPad Prism 10.6.1. (For interpretation of the references to colour in this figure legend, the reader is referred to the Web version of this article.)

moisture-sensitive compounds were performed under a nitrogen atmosphere using dried glassware and syringes techniques to transfer solutions. Nuclear magnetic resonance (^{1}H NMR, ^{13}C NMR) spectra were recorded using a Bruker Advance III 400 MHz spectrometer in DMSO-d_6. Chemical shifts are reported in parts per million (ppm) and the coupling constants (*J*) are expressed in Hertz (Hz). Splitting patterns are designated as follows: s, singlet; d, doublet; t, triplet; q, quartet; m, multiplet; dd, doublet of doublets; bs, broad singlet; ap s, apparent singlet; ap d, apparent doublet; ap t, apparent triplet; ap q, apparent quartet. The assignment of exchangeable protons (O*H* and N*H*) was confirmed by the addition of D_2O. Analytical thin-layer chromatography (TLC) was carried out on Merck silica gel F-254 plates. Flash chromatography purifications were performed on Merck silica gel 60 (230–400 mesh ASTM) as the stationary phase and methanol/dichloromethane (MeOH/DCM) or

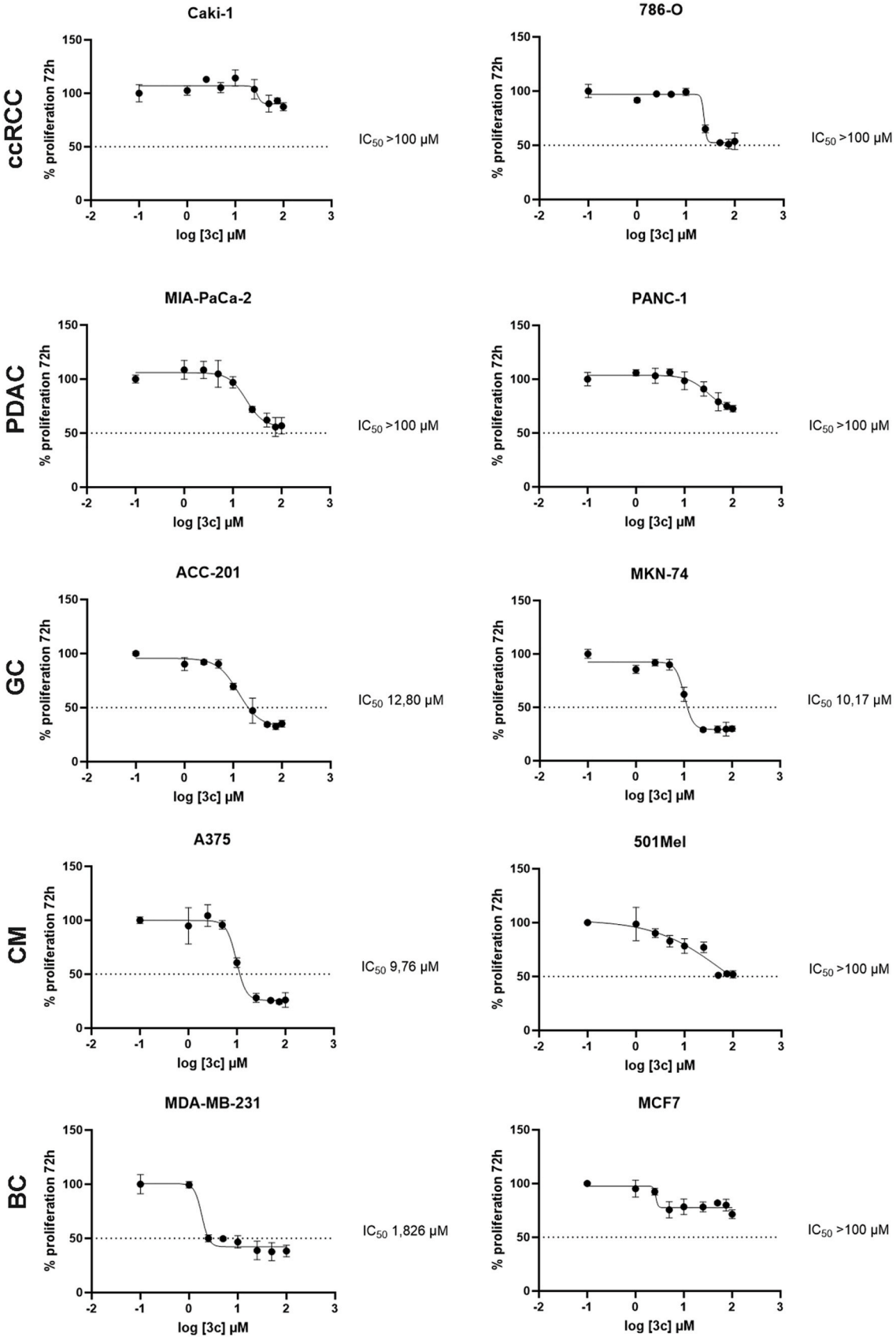

Fig. 4. Proliferation curves by MTT assay of tumor cells at 72 h of the treatment with increasing doses of **3c** compound. The calculated IC_{50} are reported on the right of each graph.

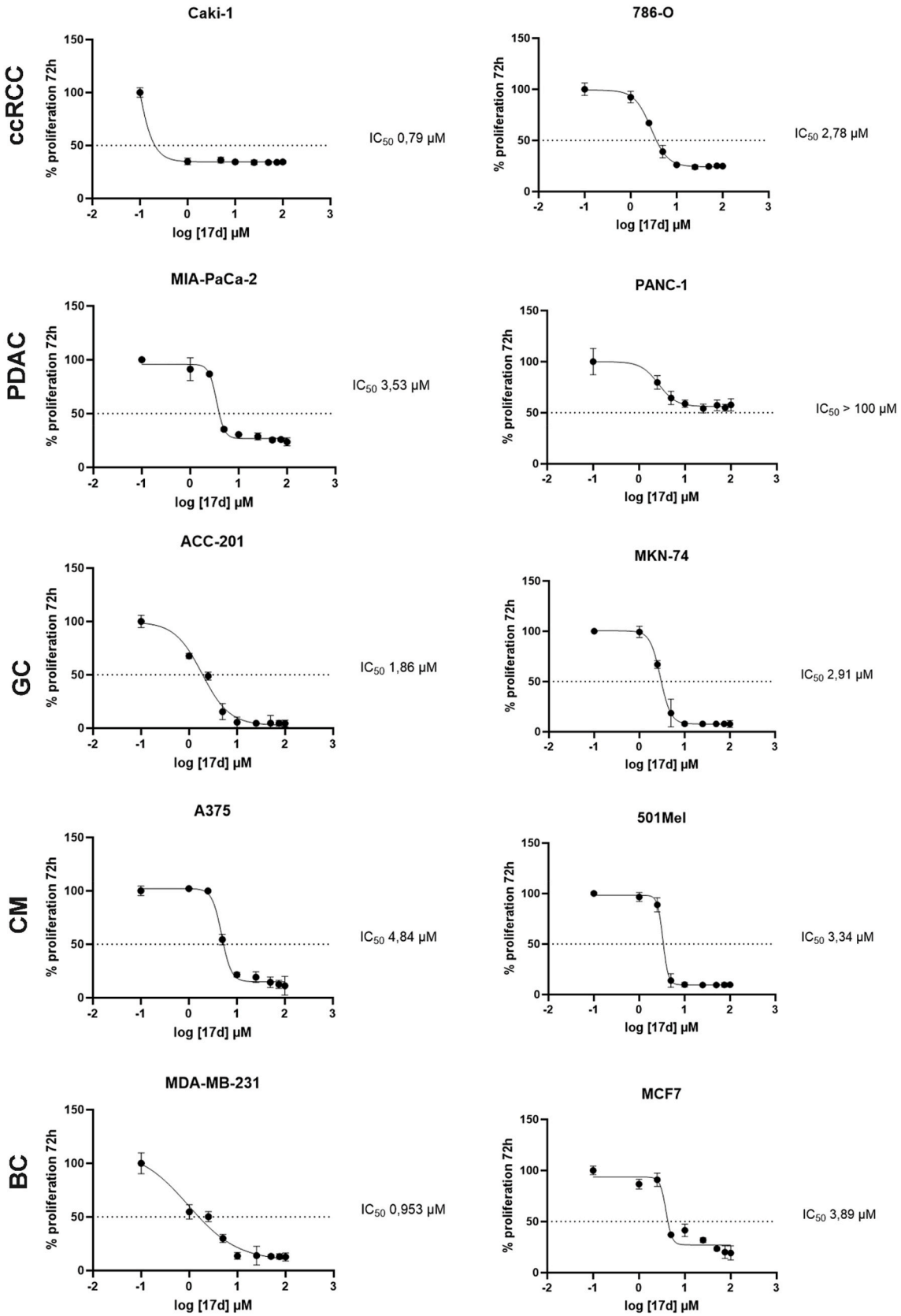

Fig. 5. Proliferation curves by MTT assay of tumor cells at 72 h of the treatment with increasing doses of **17d** compound. The calculated IC_{50}s are reported on the right of each graph.

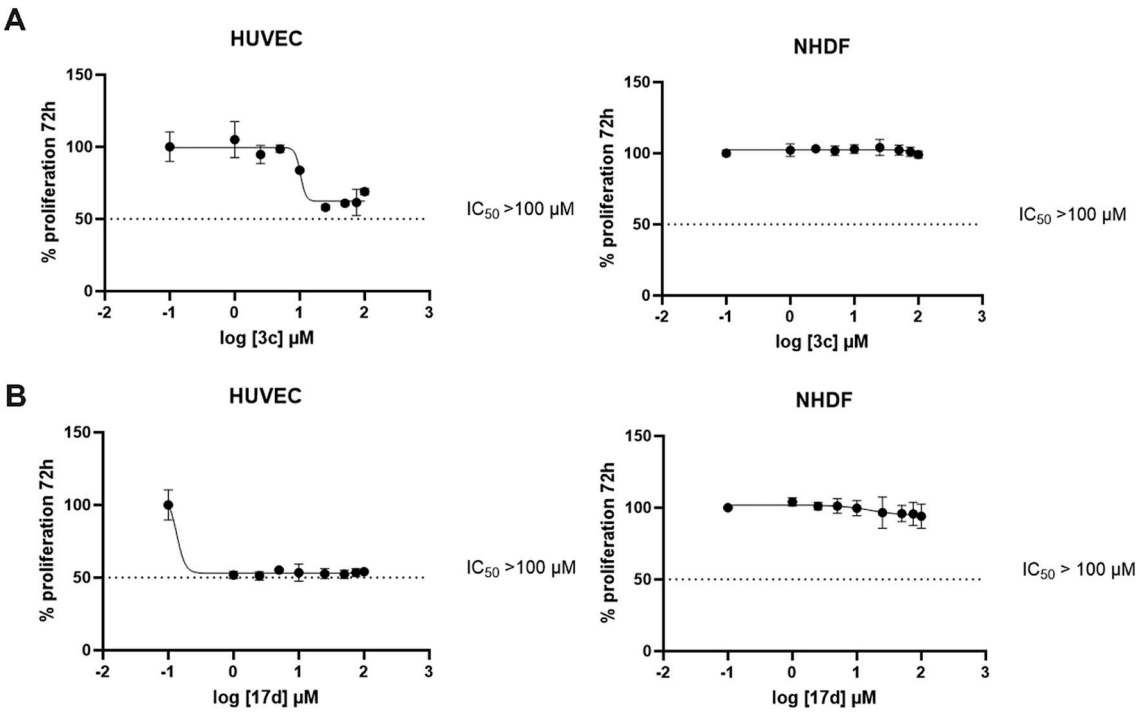

Fig. 6. Proliferation curves by MTT assay of normal human vascular endothelial cells (HUVEC) and normal human dermal fibroblasts (NHDF) cells at 72 h of the treatment with increasing doses of **3c** or **17d** compounds.

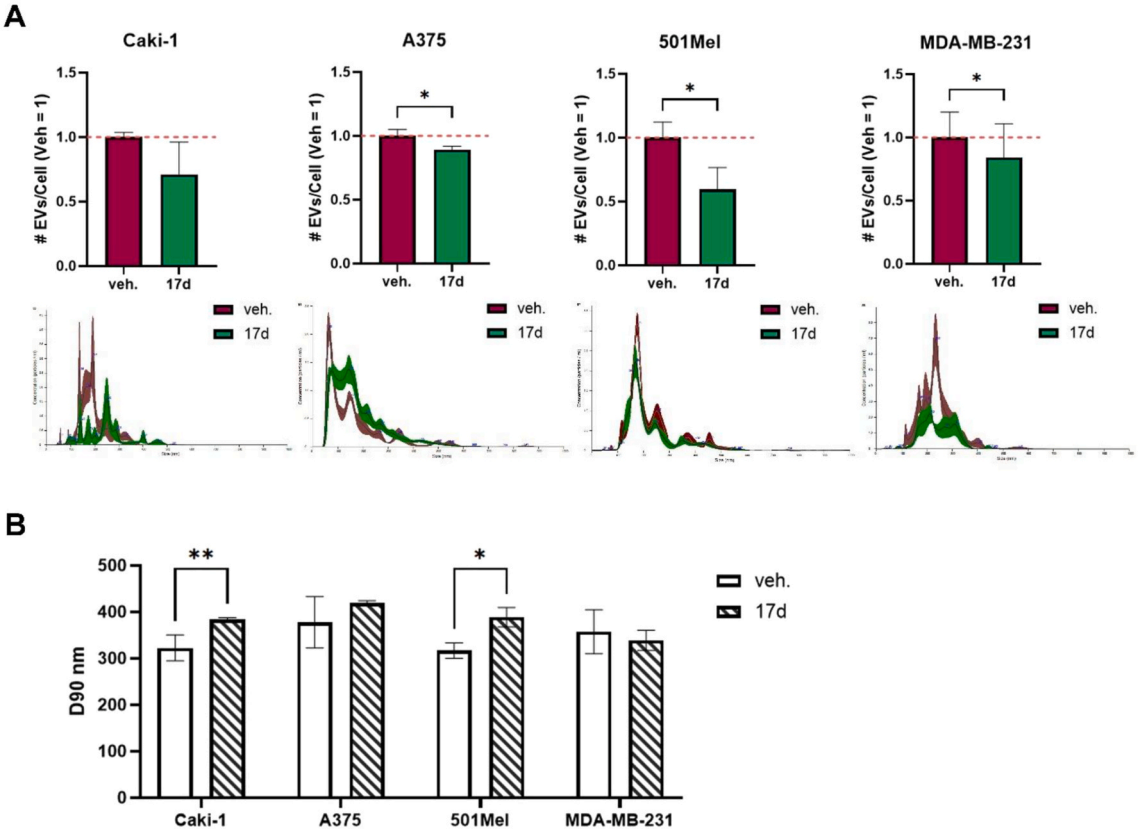

Fig. 7. Quantification charts and representative Nanosight plots of extracellular vesicles (EV) release by ccRCC Caki-1, CM A375 and 501Mel, and BC MDA-MB-231 cells treated for 24 h with the relative IC_{50} dose of **17d** compound (**A**). Quantification chart of D90 value of EV derived from vehicle or **17d** treated cells (**B**).

ethyl acetate/hexane (EtOAc/Hex) were used as eluents. The solvents used in Mass Spectra (MS) measures were acetone, acetonitrile (Chromasolv grade), and 56 mQ H_2O 18 MΩ, obtained from Millipore's Simplicity system (Milan-Italy). The mass spectra were obtained using a Varian 1200L triple quadrupole system (Palo Alto, USA) equipped by Electrospray Source (ESI) operating in both positive and negative mode. Stock solutions of analytes were prepared in acetone at 1.0 mg/mL and stored at 4 °C. Working solutions of each analyte were freshly prepared by diluting stock solutions in a mixture of mQ H_2O/ACN 1/1(v/v) up to a concentration of 1.0 μg mL^{-1}. The mass spectra of each analyte were acquired by introducing, via syringe pump at 10 L min^{-1}, the working solution. RawQdata were collected and processed by Varian Workstation Vers. 6.8. Compounds **4, 5a-d**, **6a-b**, **7a-d**, **8**–**10**, **11a-c**, **12a-c**, **13a-c**, **14**, **15**, **16a-d** and **17a-d** were obtained as previously reported [18].

4.2. General procedure for the synthesis of ureido derivatives 3a-d

1-(4-(((2*R*,4*S*)-2-((1*H*-Imidazole-1-yl)methyl)-2-(2,4-dichlorophenyl)-1,3-dioxolan-4-yl)methoxy)phenyl)piperazine (**1**) (1.0 eq.) and the appropriate carbamate (**2a-c**) or 7-isothiocyanato-4-methyl-2*H*-chromen-2-one (**2d**) (1.0 eq.) were dissolved in acetonitrile (4 mL). The reaction mixture was stirred at reflux temperature overnight. A control via TLC was performed to assure the complete consumption of the starting materials. The reaction was quenched with H_2O and the precipitate was filtered off under vacuum, washed with Et_2O and H_2O, then dried on air. A purification via silica gel flash chromatography was performed to afford the pure products.

4.2.1. 4-(4-(((2R,4S)-2-((1H-Imidazole-1-yl)methyl)-2-(2,4-dichlorophenyl)-1,3-dioxolan-4-yl)methoxy)phenyl)-N-(2-oxo-2H-chromen-6-yl)piperazine-1-carboxamide (3a)

Yellow solid 81 % yield; ^{1}H NMR (DMSO-d_6, 400 MHz): 8.88 (1H, s, N*H*, exchange with D_2O), 8.08 (1H, d, J = 9.60 Hz), 7.92 (1H, d, J = 2.48 Hz), 7.67 (1H, dd, J = 9.03 Hz; J = 2.52 Hz), 7.61 (1H, d, J = 8.48 Hz), 7.52 (1H, s), 7.50 (1H, dd, J = 8.44 Hz; J = 2.07 Hz), 7.36 (1H, d, J = 9.00 Hz), 7.19 (1H, t, J = 7.88 Hz), 7.06 (1H, s), 6.99 (1H, d, J = 9.08 Hz), 6.86 (2H, d, J = 2.56 Hz), 6.79 (2H, ap t, J = 7.96 Hz), 6.50 (1H, d, J = 9.52 Hz), 4.57 (2H, q, J = 11.24 Hz), 4.38 (1H, m), 3.90 (1H, t, J = 5.03 Hz), 3.69 (2H, m), 3.65 (4H, m), 3.55 (1H, m), 3.08 (4H, m). ^{13}C NMR (DMSO-d_6, 100 MHz): 161.1, 155.8, 153.0, 149.5, 146.5, 145.4, 139.4, 137.9, 136.1, 135.4, 133.3, 131.5, 131.0, 128.5, 128.2, 124.9, 122.0, 119.4, 119.0, 118.7, 117.1, 116.0, 108.6, 75.7, 68.9, 67.6, 51.5, 50.6, 44.6, 31.6; ESI-HRMS (*m/z*) calculated for $[M+H]^+$ ion species $C_{34}H_{31}Cl_2N_5O_6$ 676.17, found 676.19.

4.2.2. 4-(4-(((2R,4S)-2-((1H-Imidazole-1-yl)methyl)-2-(2,4-dichlorophenyl)-1,3-dioxolan-4-yl)methoxy)phenyl)-N-(2-oxo-4-(trifluoromethyl)-2H-chromen-7-yl)piperazine-1-carboxamide (3b)

Yellow solid 32 % yield; ^{1}H NMR (DMSO-d_6, 400 MHz): 9.30 (1H, s, N*H*, exchange with D_2O), 7.82 (1H, s), 7.71 (1H, s), 7.65 (1H, d, J = 8.32 Hz), 7.61 (2H, d, J = 8.32 Hz), 7.52 (1H, s), 7.48 (1H, dd, J = 8.47 Hz; J = 1.76 Hz), 7.05 (1H, s), 6.99 (2H, d, J = 8.88 Hz), 6.85 (4H, m), 4.57 (2H, q, J = 10.99 Hz), 4.38 (1H, m), 3.91 (1H, t, J = 7.46 Hz), 3.68 (4H, m), 3.58 (1H, m), 3.11 (4H, m), 2.12 (2H, s); ^{13}C NMR (DMSO-d_6, 100 MHz): 159.7, 155.7, 155.0, 153.0, 146.5, 140.5, 139.4, 136.1, 135.3, 133.3, 131.5, 131.0, 129.9 (J^1_{C-F} = 300.88 Hz), 128.5, 128.1, 125.8, 122.0, 118.7, 117.0, 116.0, 114.0 (J^2_{C-F} = 25.8 Hz), 108. 6, 107.6, 106.6, 75.5, 68.7, 67.6, 51.5, 50.6, 44.7, 31.5; ESI-HRMS (*m/z*) calculated for $[M+H]^+$ ion species $C_{35}H_{30}Cl_2F_3N_5O_6$ 744.15, found 744.18.

4.2.3. 4-(4-(((2R,4S)-2-((1H-Imidazole-1-yl)methyl)-2-(2,4-dichlorophenyl)-1,3-dioxolan-4-yl)methoxy)phenyl)-N-(4-methyl-2-oxo-2H-chromen-7-yl)piperazine-1-carboxamide (3c)

White solid 91 % yield; ^{1}H NMR (DMSO-d_6, 400 MHz): 9.12 (1H, s, N*H*, exchange with D_2O), 7.72 (1H, d, J = 1.96 Hz), 7.69 (2H, m), 7.61 (1H, d, J = 8.48 Hz), 7.53 (2H, m), 7.49 (1H, dd, J = 8.48 Hz; J = 1.99 Hz), 7.05 (1H, s), 6.99 (2H, d, J = 9.00 Hz), 6.86 (2H, s), 6.84 (1H, s), 6.24 (1H, s), 4.57 (2H, q, J = 11.11 Hz), 4.38 (1H, m), 3.91 (1H, t, J = 7.52 Hz), 3.68 (6H, m), 3.57 (1H, m), 3.10 (4H, m), 2.43 (3H, s); ^{13}C NMR (DMSO-d_6, 100 MHz): 161.1, 154.6, 154.1, 153.0, 146.5, 145.3, 139.4, 136.1, 135.3, 133.2, 131.5, 131.0, 128.5, 128.2, 126.3, 122.0, 118.7, 116.2, 116.0, 114.5, 112.3, 108.6, 106.1, 75.5, 68.7, 67.6, 51.5, 50.6, 44.7, 42.9, 18.9; ESI-HRMS (*m/z*) calculated for $[M+H]^+$ ion species $C_{35}H_{33}Cl_2N_5O_6$ 690.18, found 690.22.

4.2.4. 4-(4-(((2R,4S)-2-((1H-Imidazole-1-yl)methyl)-2-(2,4-dichlorophenyl)-1,3-dioxolan-4-yl)methoxy)phenyl)-N-(4-methyl-2-oxo-2H-chromen-7-yl)piperazine-1-carbothioamide (3d)

Yellow solid 63 % yield; ^{1}H NMR (DMSO-d_6, 400 MHz): 9.81 (1H, bs, N*H*, exchange with D_2O), 7.72 (2H, m), 7.61 (1H, d, J = 8.48 Hz), 7.52 (1H, s), 7.50 (1H, dd, J = 8.70 Hz; J = 1.89 Hz), 7.45 (2H, d, J = 9.00 Hz), 7.06 (1H, s), 6.99 (2H, d, J = 8.96 Hz), 6.85 (3H, m), 6.32 (1H, s), 4.57 (2H, q, J = 11.20 Hz), 4.38 (1H, m), 4.08 (4H, m), 3.90 (1H, t, J = 7.50 Hz), 3.69 (2H, m), 3.56 (1H, dd, J = 10.13 Hz; J = 5.24 Hz), 3.18 (4H, m), 2.45 (3H, s); ^{13}C NMR (DMSO-d_6, 100 MHz): 197.5, 181.8, 161.0, 154.1, 153.9, 152.9, 146.0, 145.7, 139.4, 136.1, 135.4, 133.3, 131.5, 131.0, 128.5, 128.2, 125.7, 122.0, 120.7, 118.5, 116.0, 113.3, 111.0, 108.6, 75.5, 68.6, 67.6, 51.5, 50.2, 49.2, 19.0; ESI-HRMS (*m/z*) calculated for $[M+H]^+$ ion species $C_{35}H_{33}Cl_2N_5O_5S$ 706.16, found 706.19.

4.2.5. General procedure for the synthesis of compounds 2a-c

In a round bottom flask, the appropriate coumarin (1.0 eq.) was dissolved in Acetone (4 mL) at 0 °C followed by the addition of K_2CO_3 (1.2 eq.). Phenyl chloroformate (1.05 eq.) was then added dropwise and the reaction mixture was stirred for 1 h at 0 °C. A control via TLC was performed to assure the complete consumption of the starting materials. The reaction mixture was evaporated under reduced pressure to remove the solvent, and water was added to quench the reaction to afford a solid, which was filtered off under vacuum, washed with Et_2O and water, then dried on air. The compounds were pure enough to be used as they are.

4.2.6. Phenyl (2-oxo-2H-chromen-6-yl)carbamate (2a)

Light yellow solid 95 % yield; ^{1}H NMR (DMSO-d_6, 400 MHz): 10.52 (1H, bs, N*H*, exchange with D_2O), 8.11 (1H, d, J = 9.60 Hz), 7.92 (1H, s), 7.69 (1H, dd, J = 8.96 Hz; J = 2.29 Hz), 7.47 (3H, m), 7.29 (3H, m), 6.53 (1H, d, J = 9.56 Hz); ^{13}C NMR (DMSO-d_6, 100 MHz): 160.9, 152.8, 151.4, 150.2, 145.2, 136.0, 130.4, 126.5, 123.7, 122.8, 122.2, 119.8, 117.8, 117.6; ESI-HRMS (*m/z*) calculated for $[M+H]^+$ ion species $C_{16}H_{11}NO_4$ 282.07, found 282.10.

4.2.7. Phenyl (2-oxo-4-(trifluoromethyl)-2H-chromen-7-yl)carbamate (2b)

Yellow solid 71 % yield; ^{1}H NMR (DMSO-d_6, 400 MHz): 10.95 (1H, bs, N*H*, exchange with D_2O), 7.73 (1H, s), 7.59 (1H, dd, J = 8.85 Hz; J = 1.86 Hz), 7.50 (3H, t, J = 8.02 Hz), 7.42 (1H, d, J = 7.72 Hz), 7.32 (2H, m), 6.94 (1H, s); ^{13}C NMR (DMSO-d_6, 100 MHz): 159.4, 155.7, 152.4, 151.1, 144.2, 130.6, 130.4, 127.4, 126.7, 126.5, 122.8, 122.1, 116.2 (q, J^1_{C-F} = 300.88 Hz), 108.9, 106.4; ESI-HRMS (*m/z*) calculated for $[M+H]^+$ ion species $C_{17}H_{10}F_3NO_4$ 350.06, found 350.10.

4.2.8. Phenyl (4-methyl-2-oxo-2H-chromen-7-yl)carbamate (2c)

Light yellow solid 95 % yield; ^{1}H NMR (DMSO-d_6, 400 MHz): 10.77 (1H, bs, N*H*, exchange with D_2O), 7.78 (1H, d, J = 9.60 Hz), 7.61 (1H, s), 7.48 (3H, m), 7.31 (3H, m), 6.30 (1H, s); ^{13}C NMR (DMSO-d_6, 100 MHz): 159.9, 153.7, 153.0, 151.5, 150.2, 142.1, 129.4, 126.1, 125.6, 121.9, 114.7, 114.4, 112.1, 104.7, 17.9; ESI-HRMS (*m/z*) calculated for $[M+H]^+$ ion species $C_{17}H_{13}NO_4$ 295.08, found 295.11.

4.2.9. Synthesis of 7-isothiocyanato-4-methyl-2H-chromen-2-one (2d)

In a dry flask, 7-amino-4-methyl-2*H*-chromen-2-one (630 mg; 3.6

mmol; 1 eq.) was dissolved in dry DCM (7 mL) followed by the addition of triethylamine (1000 μL; 7.2 mmol; 2 eq.) at 0 °C. Thiophosgene (356 μL; 4.7 mmol; 1.3 eq.) was then added dropwise. The cooling bath was removed and the reaction mixture was stirred for 30 min at room temperature. A control via TLC was performed to assure the complete consumption of the starting materials. The reaction was quenched with HCl 1 M and the product was extracted with DCM. The organic layer was dried over Na_2SO_4 and evaporated under reduced pressure. Compound **2d** was pure enough to be used as it is. Red-brown solid 94 % yield; ^{1}H NMR (DMSO-d_6, 400 MHz): 7.87 (1H, d, J = 8.49 Hz), 7.59 (1H, d, J = 2.00 Hz), 7.48 (1H, dd, J = 8.47 Hz; J = 2.02 Hz), 6.48 (1H, d, J = 1.15 Hz), 2.47 (3H, d, J = 1.14 Hz); ^{13}C NMR ($CDCl_3$, 125 MHz): 160.3, 154.4, 152.0, 139.1, 134.9, 126.4, 122.4, 119.4, 115.6, 114.2, 19.3; ESI-HRMS (m/z) calculated for $[M+H]^+$ ion species $C_{11}H_7NO_2S$ 218.02, found 218.05.

4.3. In vitro carbonic anhydrase inhibition assay

The CA-catalyzed CO_2 hydration activity measurement was performed on an Applied Photophysics stopped-flow instrument [19] using phenol red, at a concentration of 0.2 mM, as a pH indicator with 20 mM HEPES (pH 7.5) as the buffer, 20 mM Na_2SO_4, and following the initial rates of the CA-catalyzed CO_2 hydration reaction for a period of 10–100 s and working at the maximum absorbance of 557 nm. The CO_2 concentrations ranged from 1.7 to 17 mM. Enzyme concentrations varied between 5 and 12 nM. For each inhibitor, six traces of the initial 5−10 % of the reaction have been used to determine the initial velocity. The uncatalyzed reaction rates were determined in the same manner and subtracted from the total observed rates. Stock solutions of inhibitor (0.1 mM) were prepared in distilled H_2O, and dilutions up to 0.01 nM were prepared. Solutions containing inhibitor and enzyme were pre-incubated for 15 min at room temperature before assay to allow the formation of the E−I complex. The inhibition constants were obtained by nonlinear least-squares methods using PRISM 3 and the Cheng–-Prusoff equation as reported earlier [20] and represent the mean from at least three different determinations. All CAs were recombinant ones and were obtained in-house [21–23].

4.4. Cell Culture

Caki-1, 786-O, MIAPaCa-2, PANC-1, A375, 501Mel, MCF-7, MDA-MB-231 were purchased from American Type Culture Collection (ATCC, Milan, Italy), ACC-201 were obtained from the Leibniz Institute (DSMZ-German Collection of Microorganisms and Cell Cultures, Braunschweig, Germany) and MKN-74 from Cytion (S.I.A.L. S.r.l., Rome, Italy). Cells were maintained in standard conditions in a humidified incubator at 37 °C at 5 % CO_2. Differential culture media were used depending on the cell line: 786-O, PANC-1, ACC-201, and MKN-74 cells were cultured in RPMI1640 (Euroclone, Milano, Italy), MIAPaCa-2, A375, 501Mel, MCF-7, and MDA-MB-231 cells were cultured in DMEM High Glucose (Euroclone), and Caki-1 cells were maintained in McCoy's 5a (Euroclone). All the media were supplemented with 10 % FBS (Euroclone) and 1 % L-glutamine (Euroclone).

4.4.1. IC_{50} assay

5×10^3/well cancer cells were plated in a 96-well plate. After 24 h, cells were treated with increasing doses of the selected drugs. 72 h later, cells were incubated for 2 h at 37 °C in the dark with 0.5 mg/mL 3-(4,5-dimethylthiazol-2-yl)-2,5-diphenyl tetrazolium bromide (MTT) in medium without phenol red. MTT was then removed, and cells were lysed in 100 μl DMSO. Absorbance was recorded at 595 nm with an automatic plate reader (Thermofisher Scientific, Italy).

4.5. In-cell western assay

This modified version of the canonical Western Blot was performed as previously reported [24]. Briefly, 2.0×10^4 cells/well were seeded into a 96-well plate, fixed with 4 % paraformaldehyde, and permeabilized through PBS 0.1 % Triton X-100. Blocked for 1 h with Immobilion Block – FL (Fluorescent Blocker, Millipore, Sigma-Aldrich, Milan, Italy), the plate was stained for 2 h with the 1:100 anti-CA IX (66243-1-Ig, Proteintech, D.B.A. Italia s.r.l., Milan, Italy) and 1:100 anti-CA XII (68224-1-Ig, Proteintech, D.B.A. Italia s.r.l., Milan, Italy) primary antibodies, and CellTag 700 Stain (LICOR) as internal loading control. Subsequently, and after three washes with PBS 0.1 % Tween, we proceeded with the staining for 1 h at room temperature with 1:1000 goat anti-mouse-800 antibody (A32730, Invitrogen, ThermoFisher Scientific, Milan, Italy). Lastly, the plate was washed in PBS 0.1 % Tween and analysed at the Odyssey Imager (LI-COR, Germany).

4.6. EVs isolation by ultracentrifugation

Cancer cells were maintained in culture for 48 h, after which 30 mL of culture supernatant was harvested and processed by ultracentrifugation according to the minimal information for studies of extracellular vesicles (MISEV) recommendations [25]. In brief, the conditioned medium was first centrifuged at 300 g for 5 min to pellet the cells, followed by centrifugation at 3000g for 30 min at 4 °C to eliminate apoptotic bodies and cellular debris. The clarified supernatant was then subjected to 100,000 g at 4 °C for 1 h to obtain both small and large EV fractions. The isolated vesicles were finally resuspended in 100 μL of PBS and used immediately for further analysis.

4.7. Cell counting

After the conditioned medium was collected for EV isolation, cells were detached by trypsinization. Briefly, monolayers were rinsed once with PBS and incubated with trypsin-EDTA at 37 °C for 1–5 min until cells detached. Trypsin was neutralized with complete medium, and cells were then counted using a Millicell Disposable Hemocytometer (Merk Life Science S.r.l., Milan Italy). Cell concentration was calculated as (average viable cells per square × dilution factor × $10^{\wedge}4$), and total viable cell number was used to normalize EV yield (EVs per cell).

4.8. Nanoparticle tracking analysis (NTA)

NTA was carried out as previously reported [26] using a NanoSight NS300 system (Malvern Panalytical, Alfatest, Milan, Italy) equipped with a 488-nm excitation laser and an automated syringe injection unit. With this platform, EV size distribution is determined using the Stokes–Einstein equation, which relates Brownian motion to hydrodynamic diameter. Samples were diluted in sterile molecular-grade PBS and transferred into 1 mL syringes in order to be analysed with an acceptable range of 20–100 particles per frame in standard conditions, including maintaining the reading temperature at 25 °C, and a syringe pump speed set at 30.

4.9. Statistical analysis

All data were obtained based on at least three independent experiments. Statistical analysis was performed with GraphPad Prism 10.6.1 software by t-test, one-way analysis of variance (ANOVA), and two-way ANOVA, as specified. Values are presented as mean ± standard deviation (SD). The p values are presented as *p < 0.05, **p < 0.01, ***p < 0.001 and ****p < 0.0001.

CRediT authorship contribution statement

Elena Andreucci: Investigation, Funding acquisition. **Alessio Biagioni:** Writing – review & editing, Writing – original draft, Methodology, Investigation, Formal analysis, Conceptualization. **Sara Peri:** Investigation. **Nunzia Di Menna:** Investigation. **Michela Pinto:**

Investigation. **Serena Martinelli:** Investigation. **Laura Papucci:** Supervision, Methodology, Formal analysis. **Lucia Magnelli:** Investigation. **Gioele Renzi:** Investigation. **Silvia Selleri:** Supervision, Methodology, Formal analysis. **Andrea Angeli:** Supervision, Methodology, Formal analysis. **Clemente Capasso:** Supervision, Methodology, Formal analysis. **Fabrizio Carta:** Writing – review & editing, Writing – original draft, Supervision, Funding acquisition, Conceptualization. **Claudiu T. Supuran:** Supervision, Methodology, Formal analysis.

Declaration of competing interest

The authors declare that they have no known competing financial interests or personal relationships that could have appeared to influence the work reported in this paper.

Acknowledgments

Fabrizio Carta (F.C.) is grateful to the European Union - Next Generation EU. National Recovery and Resilience Plan (NRRP) - M4C2 Investment 1.5 - Research Programme ECS_00000017 - CUP.

B83C22003920001 for financial support; Elena Andreucci (E.A.) was supported by the Fondazione Associazione Italiana per la Ricerca sul Cancro (AIRC) fellowship for Italy; Alessio Biagioni (A.B.) was supported by the Accademia dei Lincei fellowship.

Appendix A. Supplementary data

Supplementary data to this article can be found online at https://doi.org/10.1016/j.ejmech.2025.118504.

Data availability

Data will be made available on request.

References

[1] N.M. Anderson, M.C. Simon, The tumor microenvironment, Curr. Biol. 16 (2020) R921–R925.
[2] J. Su, Y. Song, Z. Zhu, X. Huang, J. Fan, J. Qiao, F. Mao, Cell-cell communication: new insights and clinical implications, Signal Transduct. Targeted Ther. 1 (2024) 196.
[3] D. Neri, C.T. Supuran, Interfering with pH regulation in tumours as a therapeutic strategy, Nat. Rev. Drug Discov. 10 (2011) 767–777.
[4] E.A. Eugenin, Role of cell-to-cell communication in cancer: new features, insights, and directions, Cancer Rep. (Hoboken) 6 (2019) e1228.
[5] G. van Niel, D.R.F. Carter, A. Clayton, D.W. Lambert, G. Raposo, P. Vader, Challenges and directions in studying cell-cell communication by extracellular vesicles, Nat. Rev. Mol. Cell Biol. 5 (2022) 369–382.
[6] C.T. Supuran, Multi- and polypharmacology of carbonic anhydrase inhibitors, Pharmacol. Rev. 1 (2025) 100004.
[7] S.-H. Lee, J.R. Griffiths, How and why are cancers acidic? Carbonic anhydrase IX and the homeostatic control of tumour extracellular pH, Cancers (Basel) 6 (2020) 1616.
[8] C.T. Supuran, Carbonic anhydrases: novel therapeutic applications for inhibitors and activators, Nat. Rev. Drug Discov. 2 (2008) 168–181.
[9] P. C McDonald, S.C. Chafe, C.T. Supuran, S. Dedhar, Cancer therapeutic targeting of hypoxia induced carbonic anhydrase IX: from bench to bedside, Cancers (Basel) 14 (2022) 3297.
[10] G. Gazzaroli, C. Tavani, S. Filiberti, M.L. Massardi, M. Turati, G. Garattini, T. S. Peat, G. Pieraccini, A. Angeli, C.T. Supuran, F. Carta, A. Giacomini, R. Ronca, An ureido-substituted benzenesulfonamide carbonic anhydrase inhibitor exerts a potent antitumor effect in vitro and in vivo, Exp. Hematol. Oncol. 1 (2025) 104.
[11] E. Andreucci, A. Biagioni, S. Peri, G. Versienti, F. Cianchi, F. Staderini, L. Antonuzzo, C.T. Supuran, E. Olivo, E. Pasqualini, L. Messerini, D. Massi, M. Lulli, J. Ruzzolini, S. Peppicelli, F. Bianchini, N. Schiavone, L. Calorini, L. Magnelli, L. Papucci, The CAIX inhibitor SLC-0111 exerts anti-cancer activity on gastric cancer cell lines and resensitizes resistant cells to 5-Fluorouracil, taxane-derived, and platinum-based drugs, Cancer Lett. 571 (2023) 216338.
[12] Y. Xia, M. Sun, H. Huang, W.-L. Jin, Drug repurposing for cancer therapy, Signal Transduct. Targeted Ther. 9 (2024) 92.
[13] N. Weng, Z. Zhang, Y. Tan, X. Zhang, X. Wei, Q. Zhu, Repurposing antifungal drugs for cancer therapy, J. Adv. Res. 48 (2023) 259–273.
[14] J.W. Greenberg, H. Kim, A.A. Moustafa, A. Datta, P.C. Barata, A.H. Boulares, A. B. Abdel-Mageed, L.S. Krane, Repurposing ketoconazole as an exosome directed adjunct to sunitinib in treating renal cell carcinoma, Sci. Rep. 1 (2021) 10200.
[15] M.A. Di Bella, S. Taverna, Extracellular vesicles: diagnostic and therapeutic applications in cancer, Biology 9 (2024) 716.
[16] X. Chen, F. Yang, Classification and nomenclature of extracellular vesicles, in: Q. Wang, L. Zheng (Eds.), Extracellular Vesicles, Springer, Singapore, 2024, pp. 3–7.
[17] K. Lopez, S.W.T. Lai, E.D.J.L. Gonzalez, R.G. Dávila, S.C. Shuck, Extracellular vesicles: a dive into their role in the tumor microenvironment and cancer progression, Front. Cell Dev. Biol. 11 (2023) 1154576.
[18] G. Renzi, A. Angeli, S. Selleri, C. Spadini, N. Mezzasalma, M.T. Hull, S.L. Kelly, C. Capasso, C.S. Cabassi, F. Carta, C.T. Supuran, Design and synthesis of ketoconazole derivatives as innovative anti-infective agents, Arch. Pharm. 7 (2025) e70062.
[19] R.G. Khalifah, The carbon dioxide hydration activity of carbonic anhydrase, J. Biol. Chem. 246 (1971) 2561–2573.
[20] E. Berrino, B. Michelet, K. Vitse, A. Nocentini, G. Bartolucci, A. Martin-Mingot, P. Gratteri, F. Carta, C.T. Supuran, S. Thibaudeau, Superacid-synthesized fluorinated diamines act as selective hCA IV inhibitors, J. Med. Chem. 67 (2024) 19460–19474.
[21] J.-Y. Winum, F. Carta, C. Ward, P. Mullen, D. Harrison, S.P. Langdon, A. Cecchi, A. Scozzafava, I. Kunkler, C.T. Supuran, Ureido-substituted sulfamates show potent carbonic anhydrase IX inhibitory and antiproliferative activities against breast cancer cell lines, Bioorg. Med. Chem. Lett 14 (2012) 4681–4685.
[22] M.Y. Mboge, B.P. Mahon, N. Lamas, L. Socorro, F. Carta, C.T. Supuran, S.C. Frost, R. McKenna, Structure activity study of carbonic anhydrase IX: selective inhibition with ureido-substituted benzenesulfonamides, Eur. J. Med. Chem. 132 (2017) 184–191.
[23] C. Federici, L. Lugini, M.L. Marino, F. Carta, E. Iessi, T. Azzarito, C.T. Supuran, S. Fais, Lansoprazole and carbonic anhydrase IX inhibitors sinergize against human melanoma cells, J. Enzym. Inhib. Med. Chem. 31 (sup1) (2016) 119–125.
[24] E. Andreucci, A. Biagioni, S. Peri, G. Versienti, F. Cianchi, F. Staderini, L. Antonuzzo, C.T. Supuran, E. Olivo, E. Pasqualini, L. Messerini, D. Massi, M. Lulli, J. Ruzzolini, S. Peppicelli, F. Bianchini, N. Schiavone, L. Calorini, L. Magnelli, L. Papucci, The CAIX inhibitor SLC-0111 exerts anti-cancer activity on gastric cancer cell lines and resensitizes resistant cells to 5-Fluorouracil, taxane-derived, and platinum-based drugs, Cancer Lett. 571 (2023) 216338.
[25] J.A. Welsh, D.C.I. Goberdhan, L. O'Driscoll, E.I. Buzas, C. Blenkiron, B. Bussolati, et al., Minimal information for studies of extracellular vesicles (MISEV2023): from basic to advanced approaches, J. Extracell. Vesicles 2 (2024) 1–84.
[26] E. Andreucci, J. Ruzzolini, F. Bianchini, G. Versienti, A. Biagioni, M. Lulli, D. Guasti, P. Nardini, S. Serratì, F. Margheri, A. Laurenzana, C. Nediani, S. Peppicelli, L. Calorini, miR-214-enriched extracellular vesicles released by acid-adapted melanoma cells promote inflammatory macrophage-dependent tumor trans-endothelial migration, Cancers (Basel) 14 (2022) 5090.